Meteorol Atmos Phys (2010) 107:33–49
DOI 10.1007/s00703-010-0067-y

ORIGINAL PAPER

Simulation of heavy precipitation episode over eastern Peninsular Malaysia using MM5: sensitivity to cumulus parameterization schemes

Ester Salimun · Fredolin Tangang · Liew Juneng

Received: 31 March 2009 / Accepted: 22 March 2010 / Published online: 20 April 2010

Abstract A comparative study has been conducted to investigate the skill of four convection parameterization schemes, namely the Anthes–Kuo (AK), the Betts–Miller (BM), the Kain–Fritsch (KF), and the Grell (GR) schemes in the numerical simulation of an extreme precipitation episode over eastern Peninsular Malaysia using the Pennsylvania State University—National Center for Atmospheric Research Center (PSU-NCAR) Fifth Generation Mesoscale Model (MM5). The event is a commonly occurring westward propagating tropical depression weather system during a boreal winter resulting from an interaction between a cold surge and the quasi-stationary Borneo vortex. The model setup and other physical parameterizations are identical in all experiments and hence any difference in the simulation performance could be associated with the cumulus parameterization scheme used. From the predicted rainfall and structure of the storm, it is clear that the BM scheme has an edge over the other schemes. The rainfall intensity and spatial distribution were reasonably well simulated compared to observations. The BM scheme was also better in resolving the horizontal and vertical structures of the storm. Most of the rainfall simulated by the BM simulation was of the convective type. The failure of other schemes (AK, GR and KF) in simulating the event may be attributed to the trigger function, closure assumption, and precipitation scheme. On the other hand, the appropriateness of the BM scheme for this episode may not be generalized for other episodes or convective environments.

E. Salimun · F. Tangang (✉) · L. Juneng
Climate and Ocean Analysis Laboratory,
Research Centre for Tropical Climate Change System (IKLIM),
Faculty of Science and Technology,
National University of Malaysia,
43600 Bangi, Selangor, Malaysia
e-mail: tangang@ukm.my

1 Introduction

Widespread floods associated with heavy precipitation episodes are common occurrences on the eastern coast of Peninsular Malaysia during the northeast monsoon season (November–January). The eastern coast of Peninsular Malaysia is situated on the western part of the Maritime Continent directly facing the southern part of the South China Sea and hence receives the direct influence of strong northeasterly winds during this period. The northeasterly winds that originate from the far north are usually cool and dry but become more moist as it travels over warmer parts of the southern South China Sea (Johnson and Houze 1987). Climatologically, the monthly rainfall in this region peaks during this period. Occasionally during boreal winter anomalously stronger northeasterly cold surges prevail over the South China Sea due the intensification of the Siberian high (e.g. Chang et al. 2005). During a cold surge episode, the northeasterly winds penetrate further south reaching the southern parts of Peninsular Malaysia and Sumatra. The heavy precipitation episode that resulted in extreme flooding in southern Peninsular Malaysia and eastern Sumatra in December 2006 and January 2007 was associated with episodes of strong cold surges penetrating further south in conjunction with other circulation features (Tangang et al. 2008). However, moisture convergence over the western part of the Maritime Continent during this period is not only determined by the cold surge but is also largely influenced by the presence or absence of the quasi-stationary Borneo vortex (Chang et al. 2005). Moisture convergence tends to be over the eastern

Peninsular Malaysia region (western Borneo) when the Borneo vortex is absent (present). However, the presence of eastward propagating disturbances associated with the Madden-Julian Oscillation (MJO) affects the interaction between the cold surge and the Borneo vortex (Chang et al. 2005). In certain conditions, the interaction between the cold surge and the Borneo vortex results in a tropical storm/tropical depression that moves westward to eastern Peninsular Malaysia and subsequently causes severe flooding. The occurrence of the rare typhoon Vamei (2001) that resulted in severe flooding in the southern region of Peninsular Malaysia was associated with such an interaction (Chang et al. 2003; Juneng et al. 2007a; Tangang et al. 2007). Another example is the heavy precipitation episode of 9–11 December 2004 that will be investigated further in this study.

The 9–11 December 2004 extreme precipitation event was considered a significant episode as it caused severe flooding in Malaysian's eastern state of Pahang with some stations recording rainfall with an intensity exceeding a 100-year return period (Juneng et al. 2007b). Understanding the mechanism and enhancing the ability to numerically forecast such an episode ahead of its landfall are important aspects in mitigating the flood disasters that it can cause. Juneng et al. (2007b) presented the results of a numerical simulation of the event and an understanding of some aspects of its mechanism. However, an issue that was not addressed in the study was the sensitivity of such a numerical simulation to various physical parameterization schemes. The focus of this study is to investigate the sensitivity of the simulation of the event to cumulus parameterization schemes using the Pennsylvania State University—National Center for Atmospheric Research Center (PSU-NCAR) Fifth Generation Mesoscale Model (MM5). The choice of a cumulus parameterization scheme is known to affect the accuracy of rainfall predictions of various convective environments and their associated surface features and evolution (e.g. Wang and Seaman 1997; Rakesh et al. 2007; Vaidya 2006; Ratnam and Cox 2006; Yang and Tung 2003; Kerkhoven et al. 2006). However, a comparative study of the cumulus parameterization schemes has yet to be conducted for heavy precipitation events over this region. Although MM5 is being replaced, the Weather Research and Forecasting (WRF) model users may still benefit from the current analysis as the selected convection schemes are also available in the WRF model. Hence, the results of this investigation may serve three purposes: first, to determine an appropriate choice of cumulus parameterization schemes that works for such an episode and second, to provide some insight into why a particular scheme works well or fails to simulate the event. The third purpose is to learn about model skill and future improvement of flood forecasting and early warning system.

2 Methodology

The simulation uses the PSU-NCAR MM5 version 3 that employs a terrain following σ-coordinate system of 24 σ-levels covering the surface up to a 50-hPa level and the first sigma level is at $\sigma = 0.995$. The simulation domain employs a double two-way nested grid setup in the horizontal with a coarse domain (45 km resolution) consisting of 116×116 grid points while the inner domain has 142×142 grid points of 15 km resolution. The domain setup is slightly different from those employed in Juneng et al. (2007b). Both the inner and outer domains are larger and shifted slightly east to ensure that the simulation captures the early-stage development of the system. Figure 1 shows the inner domain with topography taken from the US Geological Survey (USGS) 5-min resolution dataset. The topography dataset was interpolated onto the model grids using a Cressman type objective analysis scheme.

2.1 Cumulus parameterization schemes

A number of cumulus parameterization schemes have been developed and in the MM5 model, users have the option to select from seven schemes including the Betts–Miller (BM) scheme (Betts and Miller 1986), the Kain Fritsch (KF) scheme (Kain and Fritsch 1993), the Grell (GR) scheme (Grell 1993; Grell et al. 1994), the Anthes–Kuo (AK) scheme (Kuo 1974; Anthes 1977), the Arakawa Schubert scheme (Arakawa and Schubert 1974), the Fritsch Chapell scheme (Fritsch and Chappell 1980), and the New Kain Fritsch scheme (Kain 2004). In this study, we consider only four schemes on the basis of their frequent use in numerical experiments. The four schemes include the AK, BM, KF, and the GR scheme. Wang and Seaman (1997) investigated these schemes for various mid-latitude convective environments and concluded that the KF scheme tended to perform better. Another earlier study by Kuo et al. (1996) found that the KF scheme performed best for the simulation of an ERICA IOP 5 storm. On the other hand, Kerkhoven et al. (2006) suggested that both the GR and BM schemes performed better at simulating a summer monsoon rainfall event over the east China regions. These studies suggest that a particular cumulus scheme may work for a particular event or convective environment, but may not work in others. The effectiveness of a particular scheme to simulate the convection depends on the design aspects of the scheme that include its triggering function, closure assumption, and precipitation scheme (e.g. Kuo et al. 1996; Kerkhoven et al. 2006). However, the assumption and simplification of a particular cumulus scheme has basically limited its effectiveness.

Here, we provide a brief overview of the four CP schemes evaluated in this study. The BM scheme is

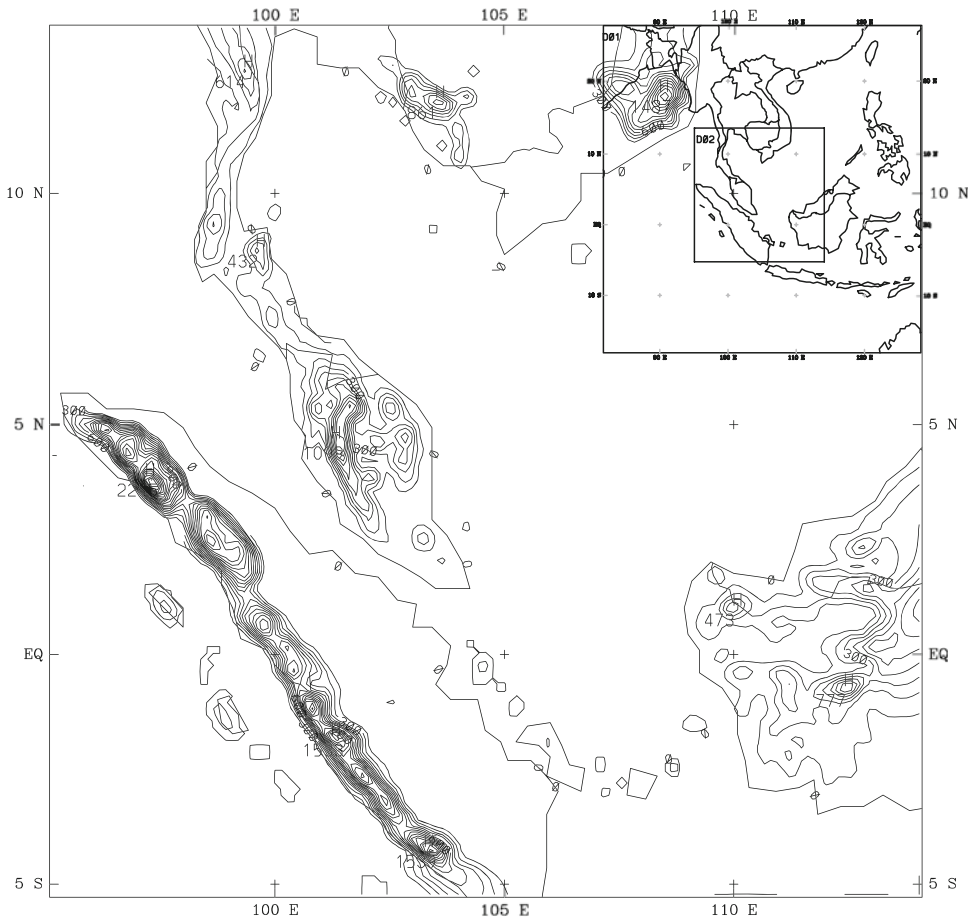

Fig. 1 Horizontal domains used in the simulations (*top right corner*) and orography in the inner domain. Isolines are drawn every 200 m

basically a penetrative adjustment scheme without a cloud model. Convectively unstable cloud layers are relaxed to a predetermined reference temperature and moisture profile (Betts and Miller 1986). The BM scheme triggers the convection whenever the atmosphere is unstable (cloud depth of 290 mb) and continues until the atmosphere stabilizes as it has no artificial constraint on the convection (Kuo et al. 1996; Kerkhoven et al. 2006). The limitation of the BM scheme includes the use of a single stable humidity profile and its lack of cloud dynamics. The AK Scheme is a modification of the Kuo (1965) scheme by Anthes (1977). The convection is determined by vertically integrated moisture convergence. This scheme partitions the grid-scale moisture convergence into two components, i.e., the production of precipitation and the moistening of the air column. Anthes (1977) set the relative contribution to the precipitation as a function of the mean relative humidity of the troposphere. The scheme does not consider cloud updrafts and downdrafts but requires available energy and sufficient moisture supply in order to trigger the convection. Kerkhoven et al. (2006) highlighted two major problems with the scheme, namely that the instability produced by energy fluxes can grow unrealistically high and that the moisture convergence is not Galilean invariant. The GR scheme is a single-cloud version of the Arakawa-Schubert scheme (Grell 1993). Its cloud model consists of 1D updraft–downdraft couplet but has no lateral entrainment. The mixing of environmental and cloud air occurs only at the top and bottom of the circulation. The closure for this scheme assumes that the rate of production of instability at the large scale equals the rate of removal of instability at the small scale (Kerkhoven et al. 2006). The KF scheme employs a 1D entraining-detraining plume without downdraft (Kain and Fritsch 1990). The convection is proportional to the available buoyant energy but the cloud depth has to be greater than 4 km in order to trigger the scheme. A more detailed overview of these cumulus schemes can be found in Kerkhoven et al. (2006) and Kuo et al. (1996). Table 1 summarizes the comparison among the convection schemes in terms of trigger function, closure assumption, and precipitation scheme.

2.2 Numerical experiments

In addition to the cumulus schemes, several other parameterization schemes were used and kept unchanged for all simulations. These include the Schultz microphysics scheme (Schultz 1995), the Blackadar scheme for the

Table 1 Comparison of different cumulus parameterization schemes in terms of convection trigger function, closure assumption, and precipitation algorithm [adopted from Kuo et al. (1996) and Kerkhoven et al. (2006)]

Cumulus scheme	Convective trigger function	Closure assumption	Precipitation scheme
Betts–Miller (BM)	Cloud depth >290 mb Stability check	Adjustment toward quasi-equilibrium reference profiles	Penetrative adjustment (no cloud model)
Grell (GR)	Lifting depth <50 mb Cloud depth >150 mb	Quasi-equilibrium assumption (the grid column is stabilized by the convection at the same rate that it is destabilized by the large-scale flow)	1D cloud model with updraft and downdraft fluxes No lateral entrainment and detrainment
Kain Fritsch (KF)	CAPE-based Cloud depth >4 km Stability check	CAPE is removed from the grid column within an convective timescale	1D mass conservative cloud model Entraining-detraining plume, with downdraft
Anthes–KUO (AK)	Vertically integrated moisture convergence > threshold value (3×10^{-5} kg m^{-2} s^{-1}) Cloud depth >300 mb Stability check	Precipitation is proportional to large scale moisture convergence	Simple 1D cloud model No downdraft

planetary boundary layer processes (Zhang and Anthes 1982), and the CCM2 radiation scheme (Kiehl et al. 1998). The choice of schemes was based on a prior experiment for which the results will be reported elsewhere. The model initial and boundary conditions were prepared by the horizontal interpolation of a 1° × 1° NCEP global analysis onto the model grids and a vertical integration to the model σ-levels. The sea surface temperature is based on the 1° × 1° weekly NOAA Optimum Interpolation version 2 SST data (Reynolds et al. 2002). The boundary conditions were imposed every 6 h. In all experiments, the model was initialized at 00UTC 9 December 2004 and integrated to 18UTC 11 December 2004 for 66 h forecasts. The predicted rainfalls were compared with the gridded observed rainfall from the Tropical Rainfall Measuring Mission (TRMM) (Huffman et al. 2007). The TRMM data compare well in terms of rainfall spatial distribution and intensity to the radar images provided by the Malaysian Meteorological Department (not shown).

2.3 Synoptic description of the event

The 9–11 December 2004 heavy precipitation episode was initiated several days earlier from a synoptic scale disturbance known as the Borneo vortex (Juneng et al. 2007b). On 5 December 2004, the vortex lingered over western Borneo, and by 6 December 2004, the system had drifted offshore and interacted with strong northeasterly winds to form an intensified closed cyclonic circulation. By 8 December 2004, the system began to drift westwards towards the eastern coast of Peninsular Malaysia. By 06UTC 9 December 2004, the center of the system was located just offshore, off the east coast of Peninsular Malaysia with a notable strengthening of surface winds of between 10 and 14 ms^{-1} over its eastern and north-northwestern quadrants (Fig. 2a). By 00UTC 10 December 2004, the center was already located over the eastern coast of Peninsular Malaysia (Fig. 2b). After landfall the system weakened considerably but continued its westward propagation, crossing Peninsular Malaysia, and by 18UTC 10 December 2004, the remnant of the system was located over the Straits of Malacca (Fig. 2c). A more detailed synoptic description of the system is presented in Juneng et al. (2007b).

The storm caused severe flooding in the east coast of Peninsular Malaysia resulting in the evacuation of more than 15,000 people and 12 causalities. However, as indicated by the spatial distribution of the 66-h accumulated rainfall from TRMM, the heaviest rainfall was basically located north of the center of the storm system with the rain band stretching in a north–south configuration from 3 to 5°N, centered at 103°E (Fig. 3). The maximum rainfall in the area exceeded 600 mm. Juneng et al. (2007b) showed that the high mountain terrain that runs from north to south in the middle of the peninsula played an important role in the distribution of the rainfall. By flattening the terrain in the inner domain, Juneng et al. (2007b) showed that the location of maximum rainfall had shifted west.

3 Results and discussion

3.1 Spatial distribution and intensity of simulated rainfall

The spatial distribution and intensity of the simulated 66-h accumulated rainfall for all cumulus experiments are

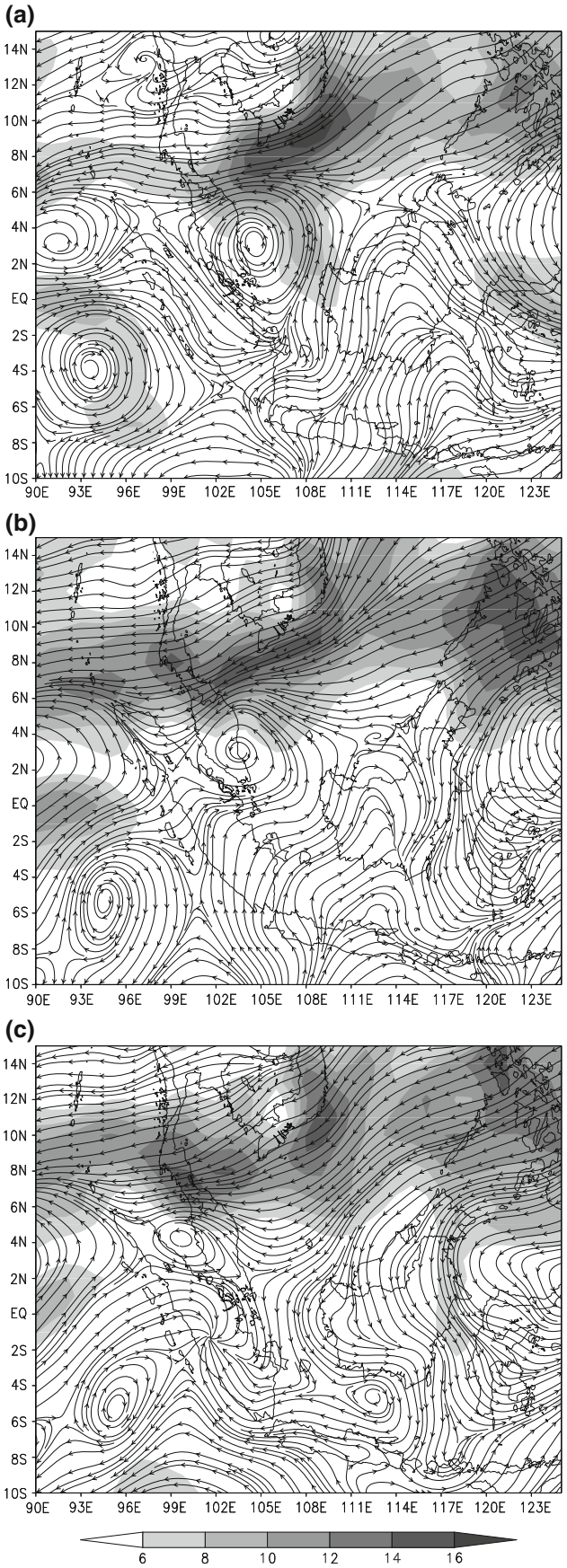

◀ **Fig. 2** 850 hPa streamline and the isotachs (*shaded*, interval 2 ms^{-1}) from the NCEP global analyses valid at (**a**) 06 UTC 9 December 2004 (**b**) 00 UTC 10 December 2004, and (**c**) 18 UTC 10 December 2004

shown in Fig. 4. All experiments show a different intensity and the distribution of simulated rainfall with that of the BM scheme shows a greater resemblance to the observed TRMM. The BM scheme is able to simulate the rain band with maximum rainfall of 500 mm, i.e., more than 80% of that observed (Fig. 4a). The simulated rainfall is also consistent with those in Juneng et al. (2007b) with minor differences that may be the result of differences in domain setup and different model integration periods. However, the other three cumulus schemes failed to produce a satisfactory pattern of rainfall distribution and intensity. The GR scheme simulated rainfall is distributed mostly north of the observed TRMM rainfall location near the Malaysia–Thailand border with a maximum rainfall of 600 mm (Fig. 4b). The KF scheme also failed to simulate rainfall over land but mostly over the South China Sea, east of eastern Peninsular Malaysia (Fig. 4c). The AK scheme simulated rainfall appeared to be widely distributed over the waters with a lowest intensity of only 220 mm (Fig. 4d). These results suggest the sensitivity of the simulated rainfall to cumulus parameterization schemes.

Figure 5a shows the temporal variation of the 3-hourly rain rates (mm/h) for the observed TRMM rainfall and the simulated values for each of the cumulus schemes averaged

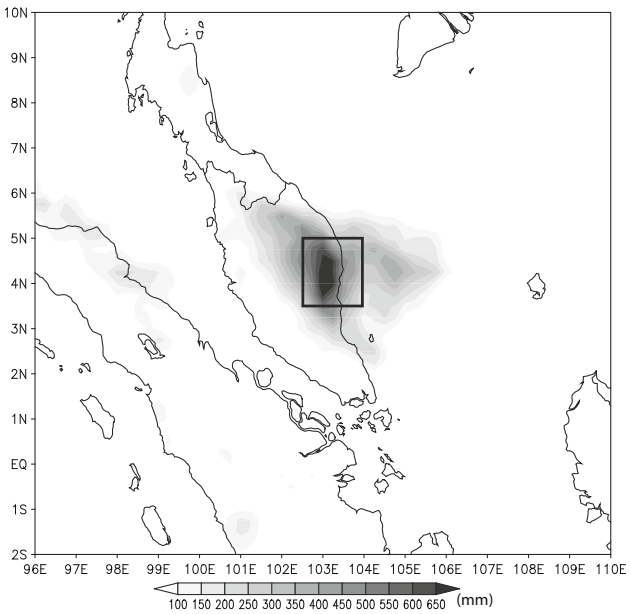

Fig. 3 Distribution of the total 66 h (00 UTC 9 December 2004–18 UTC 11 December 2004) accumulated rainfall computed from TRMM 3-hourly product. The *box* indicates the area (3.5–5°N, 102.5–104°E) where accumulated rainfall is to be computed for subsequent figures

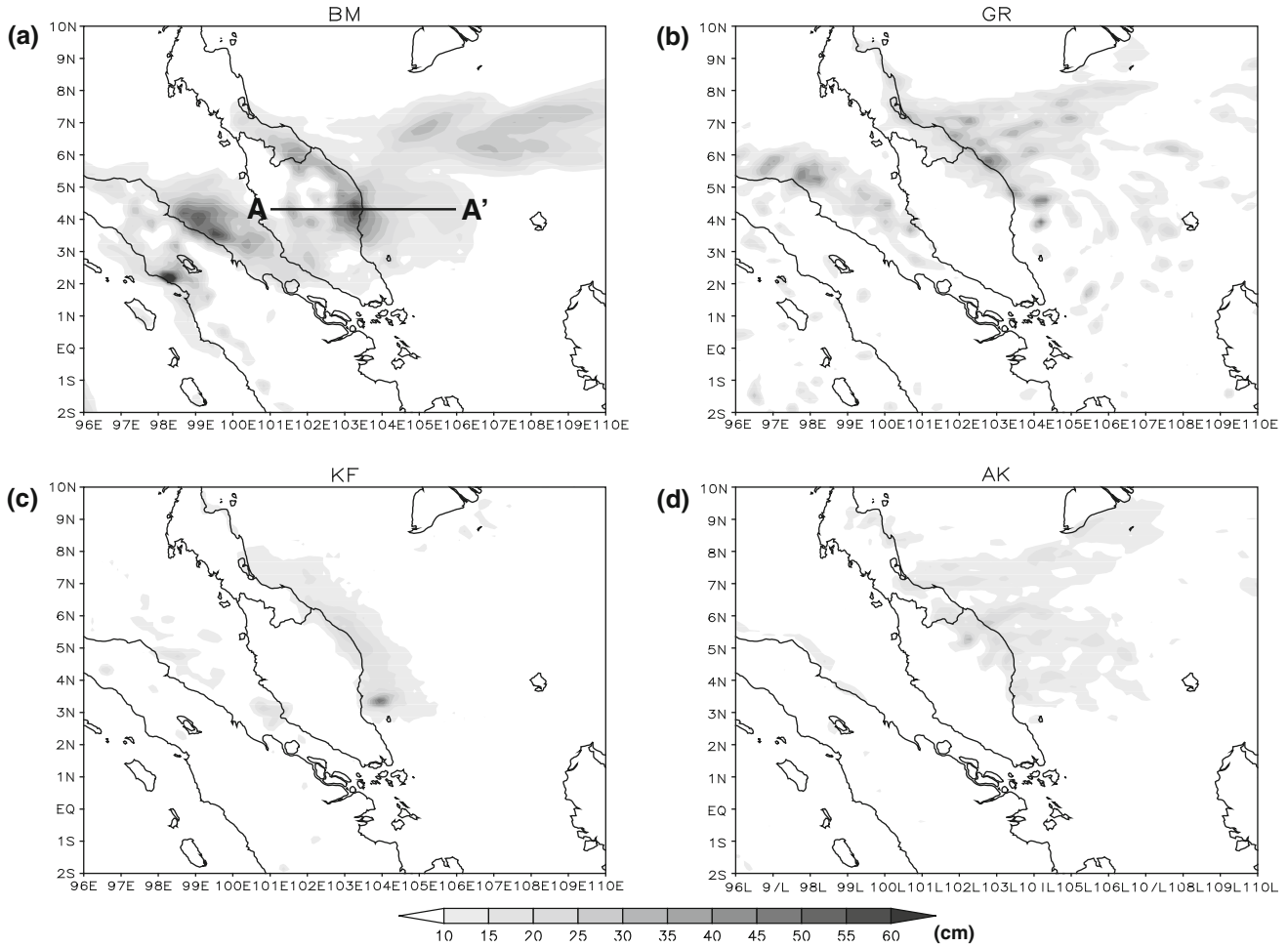

Fig. 4 Distribution of the total 66 h (00 UTC 9 December 2004–18 UTC 11 December 2004) simulated accumulated rainfall for (**a**) BM, (**b**) GR, (**c**) KF and (**d**) AK. The AA′ line indicates the transect used for vertical cross-section in Fig. 7

over an area of 3.5–5°N, 102.5–104°E; the box shown in Fig. 3. The extreme rainfall episode started in the early hours of 9 December 2004 and peaked 12–15 h later. Several hours thereafter, the intensity of the rainfall episode began to decline, but by 12 UTC 10 December 2004 the rainfall intensity started to increase again due to a secondary maximum. The evolution of the rainfall episode is captured well by the simulation with the BM cumulus scheme except that it has a somewhat lower intensity. The other cumulus schemes failed to capture the evolution of the rainfall episode. Table 2 shows the Root Means Square Error (RMSE) together with its systematic and unsystematic portions (RMSEs and RMSEu) between observed and predicted values of the 3-hourly rainfall rates. The RMSEs and RMSEu portions were computed based on Willmott (1982). Consistent with Fig. 5a, at 06 UTC 09 December 2004, there was no difference in the RMSE values among all the cumulus schemes. However, at later stages of 00 UTC 10 and 18 UTC 10 December 2004, the BM simulated rainfall has a significantly lower RMSE when compared with other schemes. The BM scheme has the lowest systematic RMSE. Willmott (1982) suggested that for a "good" model, the systematic error should approach zero while the unsystematic difference converges to the RMSE. Hence the relatively lower RMSEs values for the BM scheme seem to suggest its better performance compared with other schemes. Indeed, based on Fig. 5b, the BM scheme is the only scheme that simulates the accumulated rainfall for the same region reasonably well, i.e., about 70% of the observed compared to only about 20% for the other three schemes.

3.2 Mean sea level pressure

Figure 6 shows the predicted mean sea level pressure (MSLP) for all the cumulus schemes as well as the NCEP MSLP interpolated to the model grids plotted for the inner domain at 00 UTC 10 December 2004 and 18 UTC 10 December 2004. Due to the coarse resolution of the NCEP MSLP and the relatively small size of the storm, the

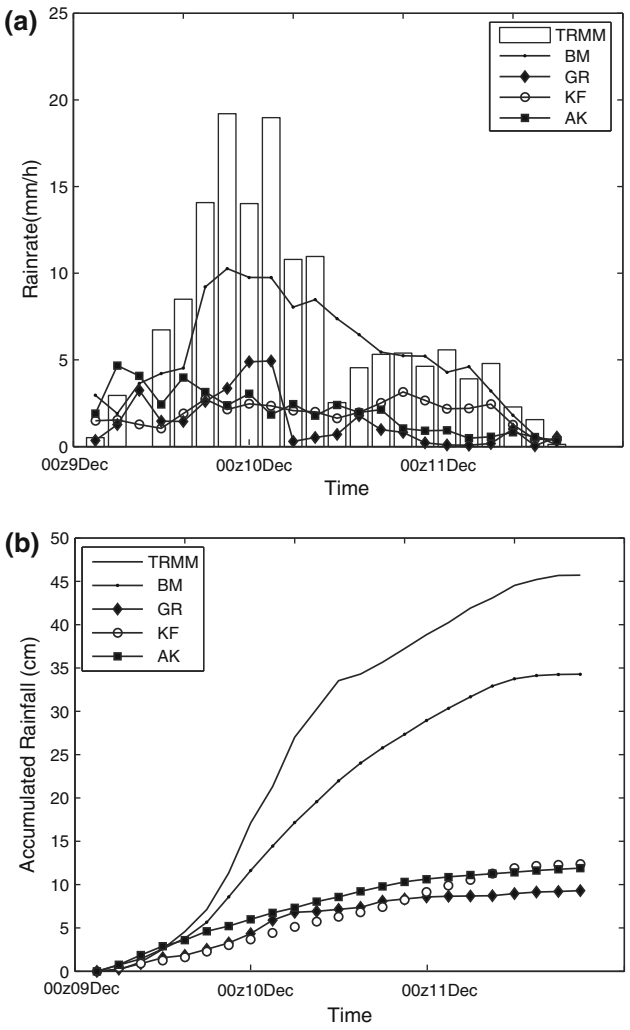

Fig. 5 **a** Three hourly time series for precipitation rate, and (**b**) 66 h time series of three hourly accumulated rainfall averaged over of 3.5–5°N, 102.5–104°E from 00 UTC 9 December to 18 UTC 11 December 2004 observed by TRMM, and obtained by using BM, KF, GR and AK cumulus schemes

horizontal structure of the storm's MSLP including the storm's center is not well resolved by the NCEP data (Fig. 6a, b). However, the horizontal structure of storm's central pressure is well simulated using the BM cumulus scheme with smoother features (Fig. 6c, d). The simulated structure clearly shows a center with minimum central pressure of 1,002 hPa. In contrast, the other cumulus schemes failed to produce a well-defined pattern of the storm's horizontal MSLP structure. For the GR scheme, a less well-developed and shallow system with central pressure of 1,008 hPa was simulated over the waters off the eastern coast of the peninsula. Several more small structures are also visible to the north of the main system (Fig. 6e, f). The horizontal MSLP structure for the KF scheme appears to be similar to that of the GR scheme. However, the spurious structures located north, simulated

Table 2 The root mean square error of differences between observed TRMM rainfall for the 3.5–5°N, 102.5–104°E region and the simulated values using various cumulus schemes (a) total RMSE, (b) systematic RMSEs and (c) unsystematic RMSEu (Unit is in cm/h)

	06z09	00z10	18z10
(a) RMSE			
BM	0.54	1.12	0.65
KF	0.46	1.66	0.73
GR	0.67	1.76	0.82
AK	0.53	1.57	0.76
(b) RMSEs			
BM	0.44	1.04	0.58
KF	0.44	1.65	0.71
GR	0.23	1.76	0.81
AK	0.47	1.54	0.73
(c) RMSEu			
BM	0.31	0.42	0.30
KF	0.14	0.16	0.17
GR	0.63	0.05	0.10
AK	0.25	0.31	0.19

in the GR scheme, were not replicated in this scheme (Fig. 6g, h). The AK scheme fails to simulate any recognizable pattern of the storm's MSLP horizontal structure (Fig. 6i, j). The BM scheme also captures the low-level circulation structures of the storm reasonably well (not shown). The simulated structures are also consistent with those of Juneng et al. (2007b) despite differences in domain setup and model integration period. However, there are notable discrepancies compared to the observed structure. Despite the well-simulated structure, the westward propagation of the simulated vortex appeared to be slower than observed. At 00UTC 10 December 2004, the center of the observed vortex is already over land (Fig. 2b) whereas the center of the simulated vortex is still over the waters. The simulated wind speeds also appear to be higher than the observed magnitudes. Over the northwest quadrant of the simulated vortex the wind speeds were between 22 and 24 ms^{-1} compared to that between 12 and 14 ms^{-1} for the observed (not shown). The performances of these schemes in simulating the storm's MSLP horizontal structure are consistent with their performances in simulating the distribution and intensity of observed rainfall as shown in Figs. 4 and 5.

3.3 Vertical structure

Figure 7 shows the east–west cross section (transect AA′ in Fig. 4) at about 4.3°N showing the vertical structures of the simulated storms at 00 UTC 10 December 2004 for the four

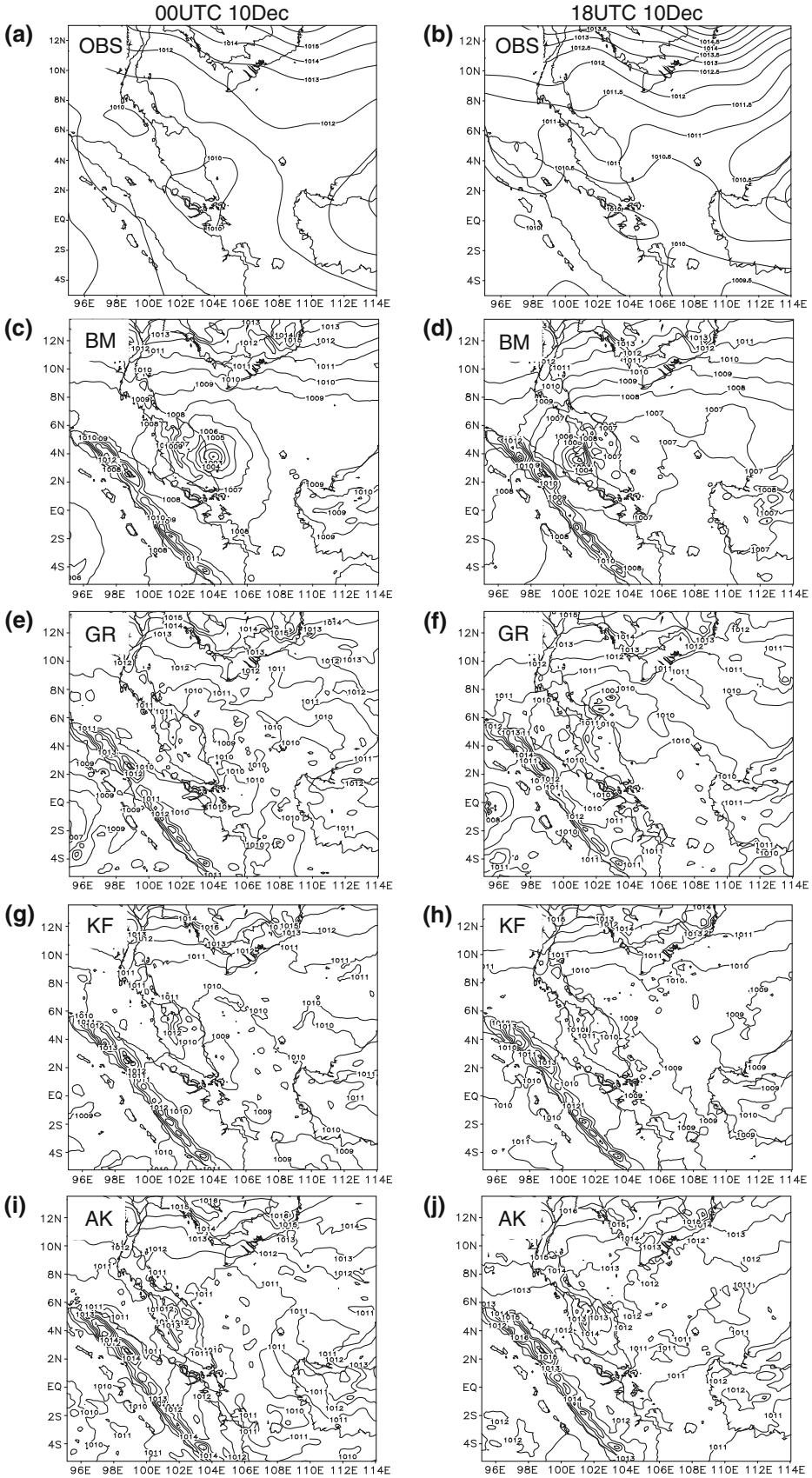

Fig. 6 Sea level pressure for (**a**, **b**) NCEP, (**c**, **d**) BM, (**e**, **f**) GR, (**g**, **h**) KF and (**i**, **j**) AK at 00 UTC 10 December 2004 and 18 UTC 10 December 2004. Unit used is hPa

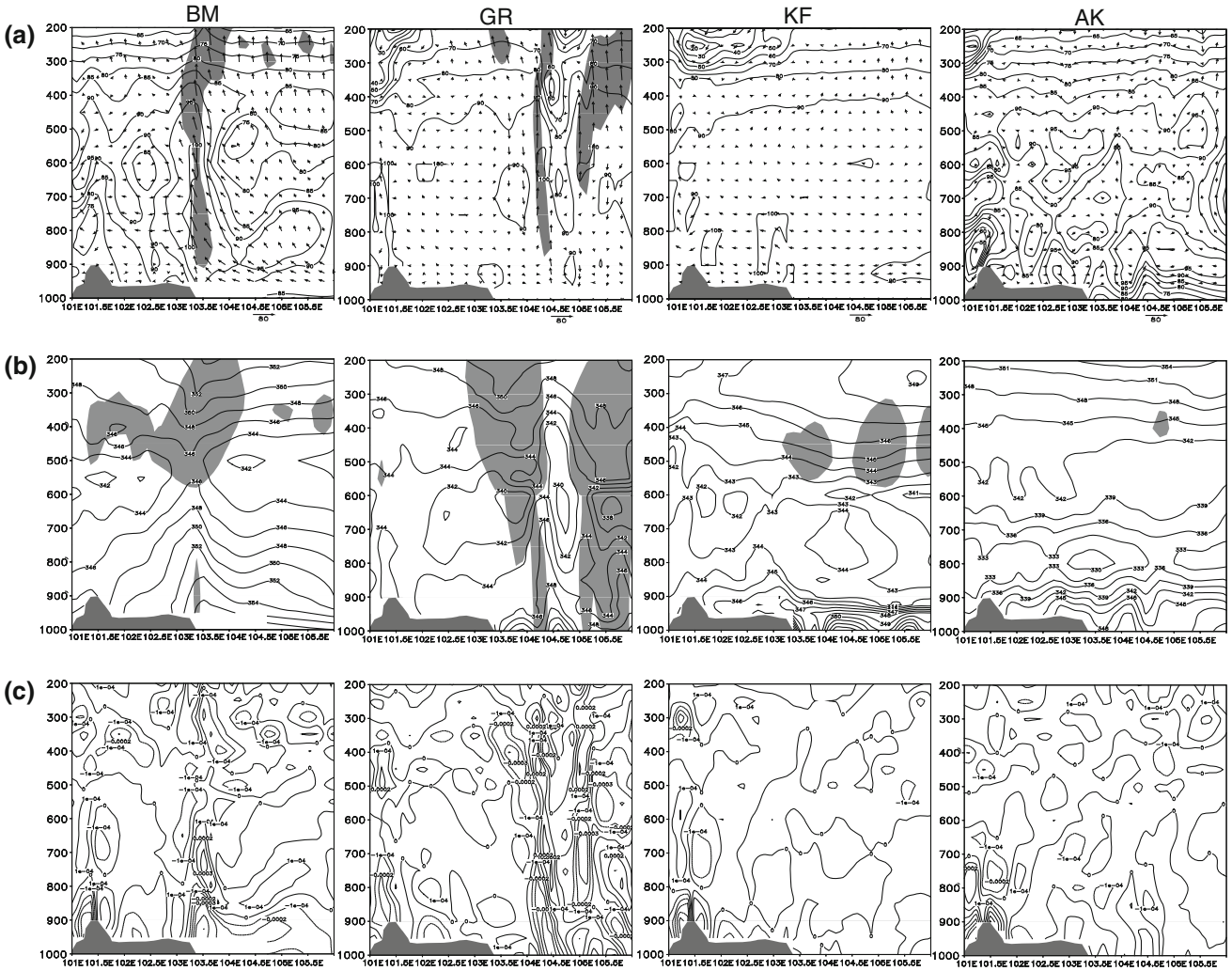

Fig. 7 Simulated vertical cross section at transect AA′ as in Fig. 4 (00 UTC 10 Dec 2004) for (**a**) wind vector (ms^{-1}) and relative humidity (%)(contour), (**b**) equivalent potential temperature (K) and (**c**) wind convergence (s^{-1}) for BM, GR, KF and AK. The *shaded area* in (**a**) is the vertical velocity value. The grayed region in (**b**) indicates the area with rain water of more than 1.5 g kg^{-1}

cumulus parameterizations. The position of the transect line is determined by the location of the observed maximum rainfall. As expected from previous results, only the BM scheme was able to simulate the vertical structure of the storm. Consistent with Juneng et al. (2007b), the strong upward motions near the center of the storm indicates strong convection (Fig. 7a of BM scheme). Strong low-level convergence is apparent from below to about the 700 hPa level. Above the 500-hPa level, the flow tends to be divergent to allow for the evacuation of the ascending air (Fig. 7c of BM scheme). As argued in Juneng et al. (2007b), the steep vertical gradient in the equivalent potential temperature (θ_e) to the east of the storm center indicates that the low-level moist air from the South China Sea with $\theta_e >$ than 350 K is the main energy source driving the system (Fig. 7b of BM scheme). The backward trajectory analysis of air parcels conducted in Juneng et al. (2007b, their Fig. 12) indicates that air parcels at 900 hPa level and above, travelling in arc-shaped trajectories, had their origins in the south-southeast region of high relative humidity and steep θ_e gradient over the South China Sea. The existence of a thermal ridge extending upwards into the level of about 400 hPa indicates the typical structure of a storm. The formation of the warm core is due to the latent heat release as the air ascends.

3.4 Convective and non-convective precipitation

In this section, we compare the convective or sub-grid scale (left column) and non-convective (right column) precipitation at 00 UTC 10 December of each cumulus parameterization scheme (Fig. 8). Consistent with previous results, significant variations can be seen among different schemes. The BM scheme produced widespread convective

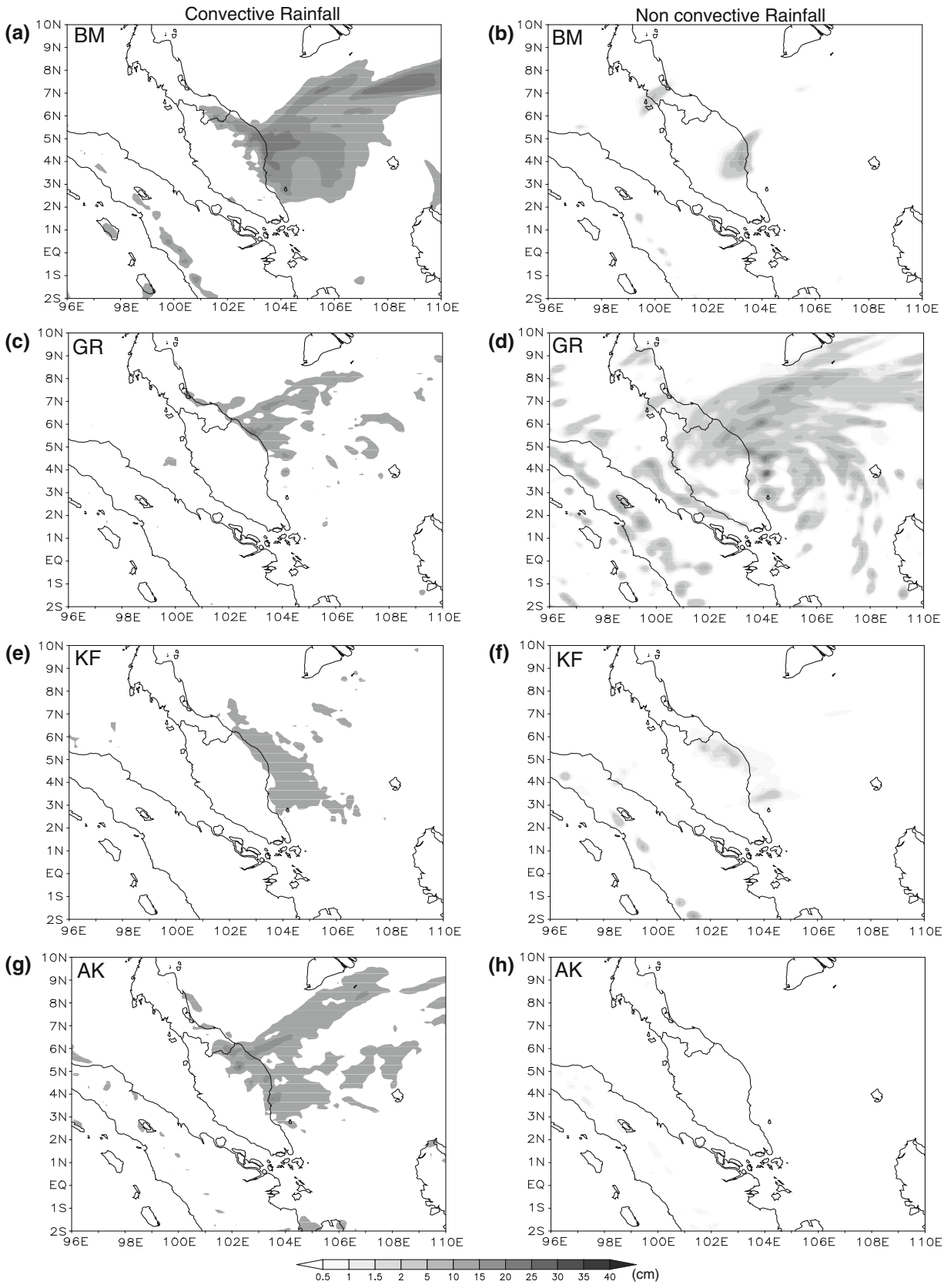

Fig. 8 Distribution of the 66-h simulated convective and non-convective rainfall at 00 UTC 10 December 2004 for BM (**a**, **b**), GR (**c**, **d**), KF(**e**, **f**) and AK (**g**, **h**). Unit used is cm

precipitation while the non-convective precipitation was confined over the area of observed maximum rainfall (Fig. 8a, b). On the other hand, the GR scheme simulated much less convective rainfall and shifted to the north (Fig. 8c),whereas non-convective precipitation spreads over a wider region (Fig. 8d). The KF Scheme produced convective precipitation at the northern part (Fig. 8e), whereas the non-convective precipitation was mainly located over land at the northern part of the peninsula (Fig. 8f). In contrast, the AK scheme exhibited convective precipitation both over the eastern coast of Peninsular Malaysia and the sea, but no non-convective precipitation (Fig. 8g, h).

Figure 9 provides the percentage of convective precipitation to the total precipitation averaged over a boxed area indicated in Fig. 3 throughout the simulation period. Interestingly, the lack of non-convective precipitation for the AK scheme was not just at 00 UTC 10 December, but throughout the simulation period. For the GR scheme, the ratios fluctuate but most of the time the values remain small indicating a higher contribution of non-convective rainfall. The BM scheme shows an interesting pattern with domination by the convective rainfall from the beginning to at about 15 h of simulation time (including 12 h spin up time) when the non-convective rainfall increases in which the ratio reaches a minimum at about 20 h of simulation time, coinciding with the time when the rainfall episode reaches the maximum. The non-convective contribution subsequently reduces and by about 35 h of simulation time, all rainfalls are of the convective type. The pattern for the KF scheme is similar to that of the BM scheme except that the period where the ratios reduce occurred slightly later. The results presented in Figs. 8 and 9 clearly show that there is a significant variation in the partitioning, intensity,

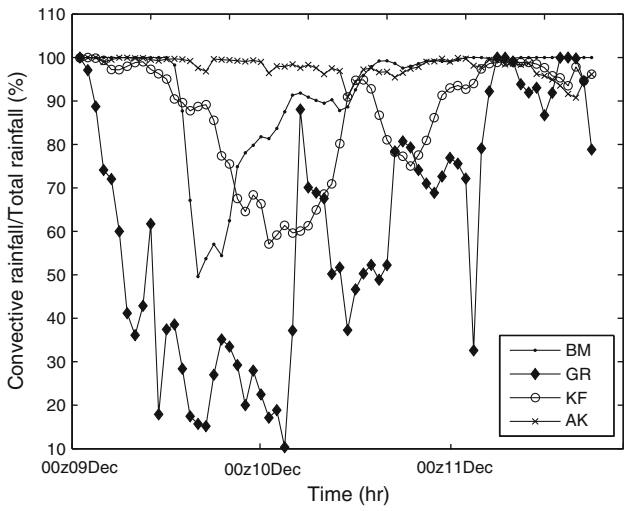

Fig. 9 Ratio of convective rainfall to the total rainfall (%) averaged over the area 3.5–5°N, 102.5–104°E for BM, KF, GR, and AK

and distribution of convective and non-convective precipitation among the schemes. Interestingly, although all experiments used the same Schultz microphysics scheme, the non-convective precipitation differed widely both in terms of intensity and spatial distribution among the schemes. Kuo et al. (1996) attributed this to the effect of convective heat and moisture transports that exert significant influences on the moisture and temperature distributions in each simulation and these affect the density and distribution of non-convective precipitation. Thorough examination of the interaction of each scheme with non-convective microphysical parameterization was not conducted in this study. However, it is worth mentioning that the behavior of both the GR and AK schemes was similar to that reported by Kuo et al. (1996). Kuo et al. (1996) argued that the limited convective precipitation simulated by the GR scheme was probably due to the fact that the precipitation efficiency parameterization determines the intensity of convective downdrafts and automatic shut-off switch. The deficiencies in the parameterizations of convective downdrafts and precipitation efficiency would result in this switch to cause the scheme to shut off too often and allows the non-convective scheme to dominate (Kuo et al. 1996). The minimal non-convective precipitation by the AK scheme could be due to the same reason provided by Kuo et al. (1996) for the Kuo Scheme since the AK scheme was basically the modified version of the Kuo Scheme. These could be related to the dependence of convective precipitation on moisture convergence and the specified convective heating profile.

3.5 Using different cumulus parameterization schemes in each domain

In this section we examine the robustness of the BM scheme by using different cumulus schemes in each domain. Figure 10 shows the intensity and spatial distribution of cumulative rainfall for the 66-h simulation. The left column indicates the results when the outer domain uses the BM scheme while the inner employs the other schemes. The right column presents the results for the reverse order. One has to be cautious when interpreting these results as this approach may introduce problems related to using different cumulus parameterization concepts simultaneously (Kerkhoven et al. 2006). Hence the comments here will be limited to identification of a general pattern of precipitation. Interestingly, when the BM scheme was used in the outer domain in conjunction with other schemes in the inner domain, the combination of these schemes failed to simulate the intensity and spatial pattern of the precipitation distribution. However, the intensity and distribution of the rainfall were reasonably simulated when the BM scheme was used for the inner

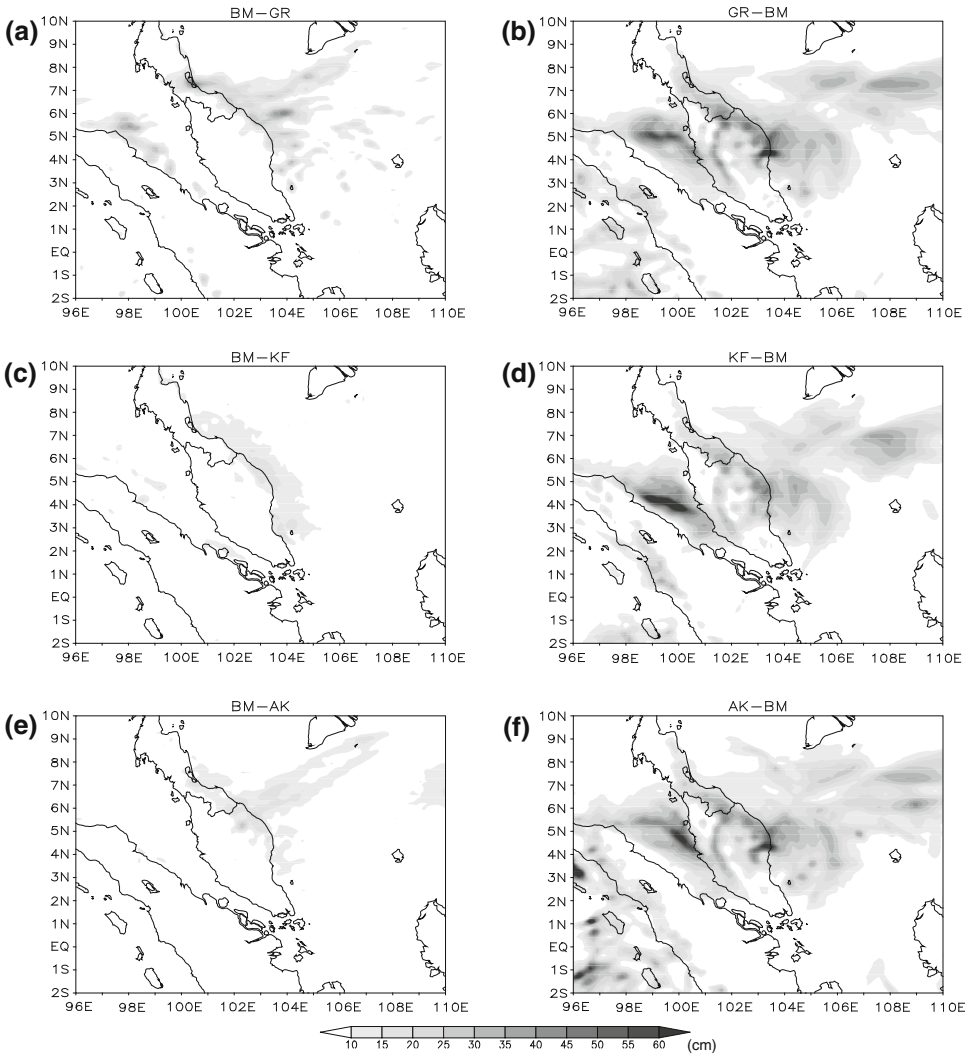

Fig. 10 Distribution of the total 66 h (00 UTC 9 December 2004–18 UTC 11 December 2004) simulated accumulated rainfall for (**a**) BM-GR, (**b**) GR-BM, (**c**) BM-KF, (**d**) KF-BM, (**e**) BM-AK, and (**f**) AK-BM

domain regardless of the scheme used for the outer domain. These results seem to suggest the robustness of the BM cumulus scheme for this episode.

3.6 Trigger functions, closure assumptions, and precipitation schemes

The overall results show the appropriateness of the BM scheme compared to other schemes for simulating the convection for this episode. The performance of these schemes may be explained by their designs, i.e., trigger functions, closure assumptions, and precipitation schemes (Table 1). Figure 11 shows the computed Convection Available Potential Energy (CAPE) from the four simulations at 00 UTC 10 Dec 2004. Generally, the CAPE values are in between low and moderate for all the simulations with an average value of about 1,000 J/kg around the east coast of Peninsular Malaysia. This suggests that the precipitation event occurred within a weak to moderate CAPE environment (at least in the model simulations). Given the weak CAPE surroundings, the triggering of deep convections in the model may be extremely sensitive to how restrictive the rules of convection triggering functions are to the instability. Figure 12 shows the height-time cross-section of the cloud water mixing ratios over the area of maximum rainfall (the boxed area indicated in Fig. 3). It is shown that both KF and AK schemes produced weak convective clouds over the rainfall area, especially after 00 UTC 10 December 2004. On the other hand, both the BM and GR schemes provide higher values of cloud water mixing ratios, suggesting more convective cloud produced by these schemes. The AK scheme uses a trigger function based on the amount of the column integrated moisture convergence which has been criticized for being physically flawed (Emanuel 1994). Furthermore, it also has a requirement of cloud depth of at least 300 mb to trigger the scheme. This implies that the instability condition is much higher for AK than other schemes for convection to be triggered (Table 1). According to Krishnamurti et al. (1983) and Das et al. (1988), it is not uncommon for the

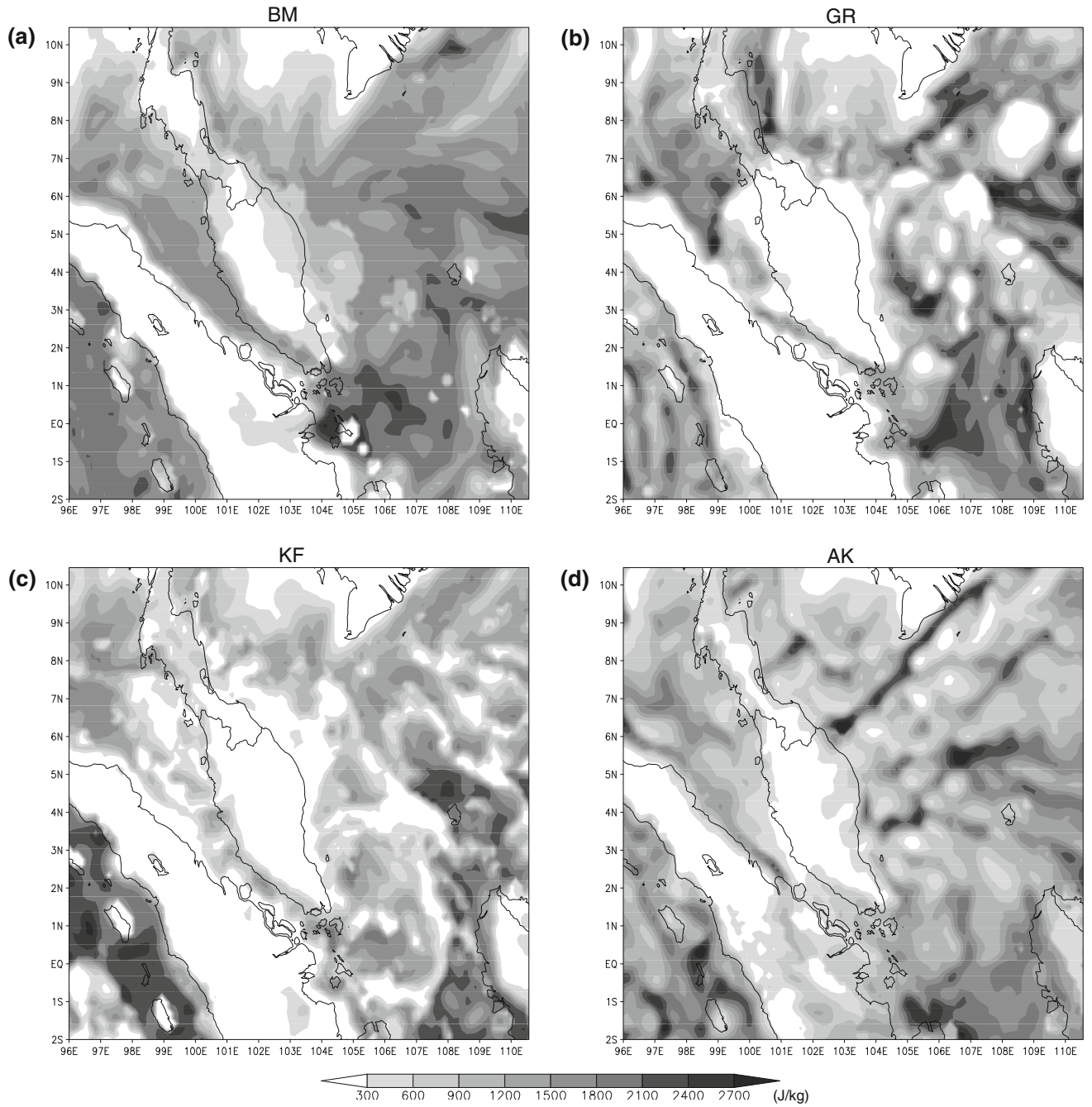

Fig. 11 Convective available potential energy at 00 UTC 10 Dec 2004 for (**a**) BM, (**b**) GR, (**c**) KF, and (**d**) AK. Unit used is (J/kg)

AK scheme to underestimate rainfall. Raymond and Emanuel (1993) also noted that numerous problems occurred when using the AK scheme. The KF scheme triggers convections when the temperature of the air parcels plus the temperature perturbation associated with the grid scale vertical velocity exceeds that of the environment temperature (Table 1). Also, the scheme requires cloud depth to be at least 4 km in order for the scheme to be triggered. Under a weak flow and low CAPE environment, these conditions may prohibit active deep convection in the model. Experiments of Kain and Fritsch (1992) suggested that the simulation of a convective weather system with the KF scheme is very sensitive to the triggering function used.

Both the BM and GR schemes produced more convective clouds as shown in Fig. 12. The GR scheme is activated when the low-level parcel is lifted no greater than 50 mb to the level of free convection and that the cloud depth is at least 150 mb (Table 1). These rules are less restrictive compared to that of BM's where the cloud depth has to be at least 290 mb. This provides more convective

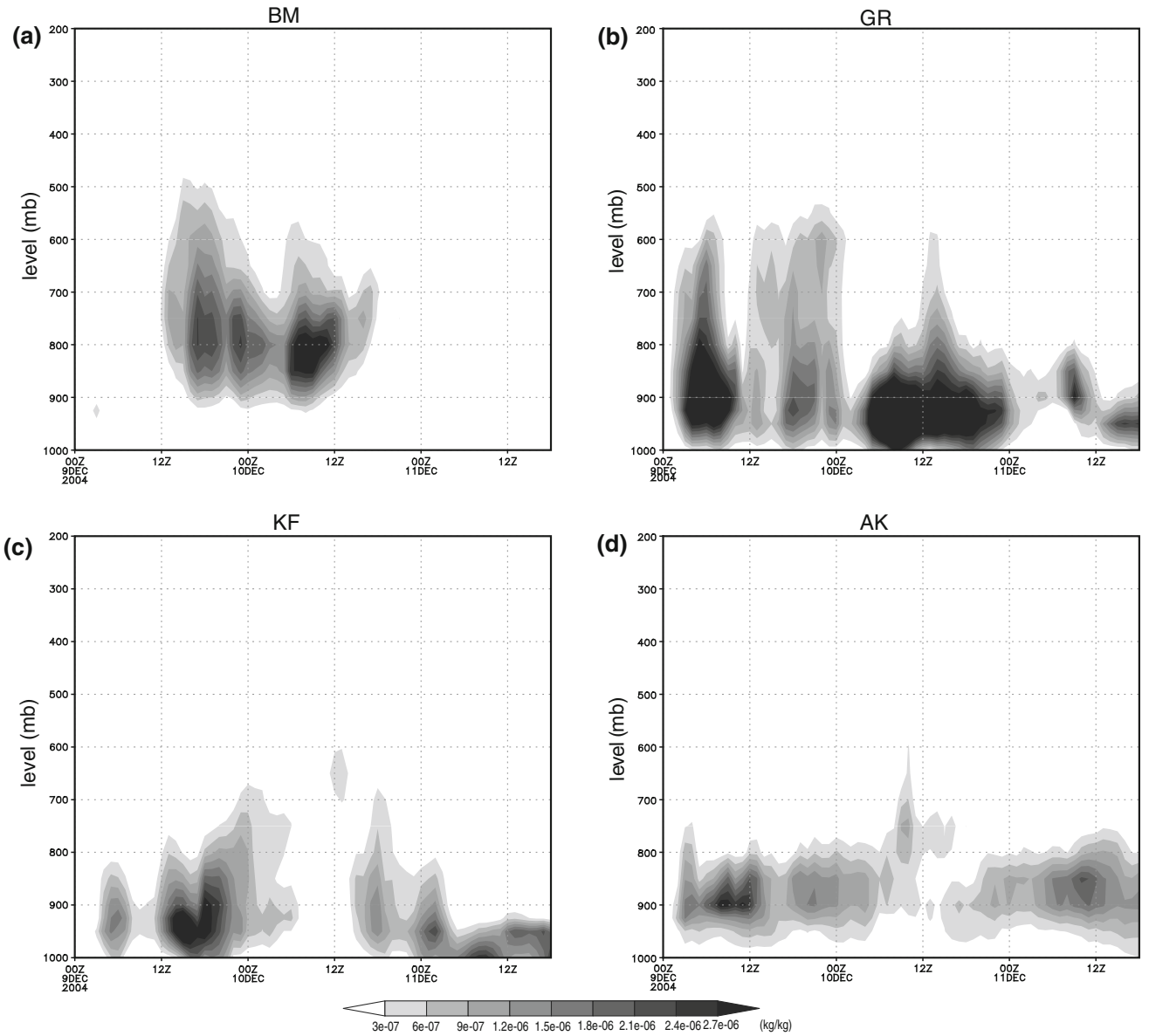

Fig. 12 Height-time cross section for cloud water mixing ratio averaged at area 3.5–5°N, 102.5–104°E for (**a**) BM, (**b**) GR, (**c**) KF, and (**d**) AK. Unit used is (kg/kg)

cloud in the GR scheme (Fig. 12b). However, the height-time cross section of the BM simulation shows a higher value of rain water mixing ratio compared to that of the GR simulation (Fig. 13). This may suggest that the BM is more effective in re-stabilizing the atmosphere instability over the region of maximum rainfall compared to the GR schemes. The deficiency may be related to the closure assumption and precipitation scheme in the GR scheme. In the GR scheme, the assumption implies that the rate at which the scheme removes instability at the sub-grid scale is equal to the rate at which the instability is produced at the resolved grid scale (Table 1). The fact that less precipitation was produced with apparent patchiness of the rainfall distribution suggests that the GR assumption and the precipitation scheme may not be appropriate or sufficient for this particular episode. In contrast, for the BM scheme, which assumes an adjustment towards a reference or predefined empirical moist adiabat profiles, the performance was more satisfactory than the more physically based schemes (KF, GR and AK). This suggests that the physics in these schemes fails to represent the convective process for this episode. However, the performance of the BM scheme may not be generalized for simulation of various atmospheric processes over the region. Our earlier

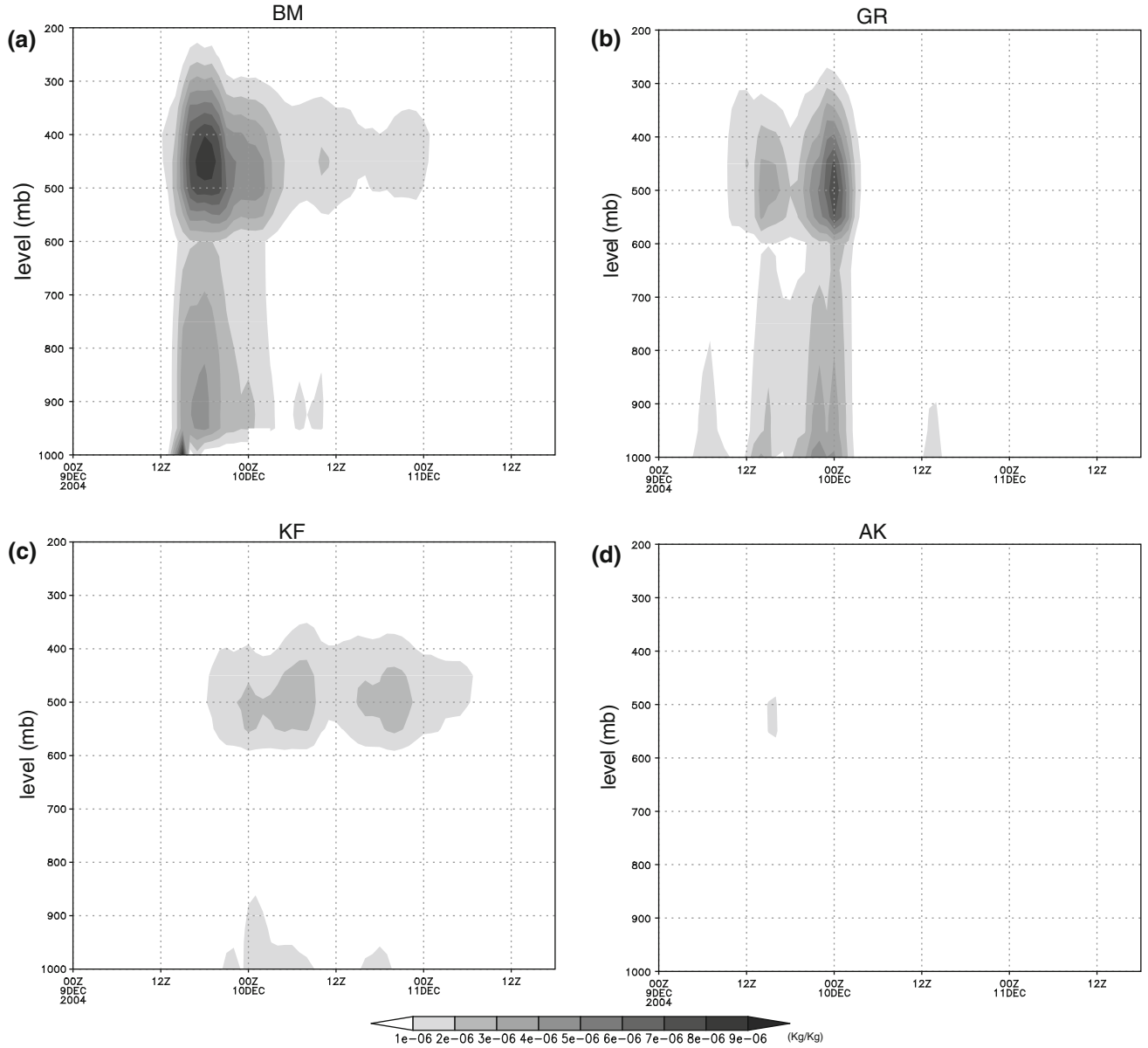

Fig. 13 Height-time cross section for rain water mixing ratio averaged at area 3.5–5°N, 102.5–104°E for (**a**) BM, (**b**) GR, (**c**) KF, and (**d**) AK. Unit used is (kg/kg)

simulation work on typhoon Vamei (2001) showed that the KF scheme provided better simulation compared to the other schemes.

4 Summary and conclusion

This study compares the performance of four cumulus parameterization schemes in the simulation of the 9–11 December 2004 extreme precipitation episode over eastern Peninsular Malaysia using the MM5 model. This is the first study conducted to investigate the simulation sensitivity of a near-equatorial convective system over the western Maritime Continent to four different cumulus parameterization schemes in MM5. In all experiments, the setups were identical except for the use of different cumulus schemes. Hence differences in the simulation results may be attributed to the sensitivity of the cumulus schemes. The simulation results indicate that the BM scheme has the edge over the other schemes. The BM scheme was able to better simulate the intensity and distribution of the rainfall. The BM's systematic RMSE is also smaller than other schemes, indicating its better performance. The horizontal and vertical structures of the storm are also well simulated by the BM simulation. The robustness of the BM scheme was also demonstrated in an experiment in which using the

scheme in the inner domain produces reasonable simulation regardless of what scheme is used at the outer domain. The BM's superior performance is attributed to its less restrictive trigger function and closure assumption. On the other hand, the failure of the other schemes (AK, GR and KF) in simulating the event can be related to their trigger function, closure assumption, and precipitation scheme. Although the understanding from the current analysis is useful, further research is required as the BM's performance for this episode may not be generalized for other events. For reliable and skillful weather and flood forecasting, and early warning system, the robustness of cumulus parameterization scheme for such extreme weather episodes over this region is crucial.

Acknowledgments This research is funded by the Malaysian Government Science Fund Grants No. 04-01-02-SF413 and 04-01-02-SF0437 and the UKM Research University Grants No. UKM-GUP-ASPL-08-05-218 and UKM-OUP_PI-34-172/2008. We would also like to thank Bob Hart of the Department of Meteorology, Penn State University for the use of the plotskew.gs GrADS script. We are grateful to the Malaysian Meteorological Department for providing us with the radar images for the episode. We are also grateful to the anonymous reviewers for their valuable comments.

References

Anthes RA (1977) A cumulus parameterization scheme utilizing a one-dimensional cloud model. Mon Wea Rev 105:270–286

Arakawa A, Schubert WH (1974) Interaction of a cumulus cloud ensemble with the large-scale environment. Part I. J Atmos Sci 31:674–701

Betts AK, Miller MJ (1986) A new convective adjustment scheme. Part II: single column test using GATE wave, BOMEX, ATEX, and Arctic air mass data sets. Q J R Meteorol Soc 112:693–709

Chang CP, Liu CH, Kuo HC (2003) Typhoon Vamei: an equatorial tropical cyclone formation. Geophys Res Lett 30:1150

Chang CP, Harr PA, Chen HJ (2005) Synoptic disturbances over the Equatorial South China Sea and western maritime continent during boreal winter. Mon Wea Rev 133:489–503

Das S, Mohanty UC, Sharma OP (1988) Study of Kuo-type cumulus parameterization during different epochs of the Asian summer monsoon. Mon Wea Rev 116:715–729

Emanuel KA (1994) Atmospheric convection. Oxford University Press, New York

Fritsch JM, Chappell CF (1980) Numerical prediction of convectively driven mesoscale pressure systems. Part I: convective parameterization. J Atmos Sci 37:1722–1733

Grell GA (1993) Prognostic evaluation of assumptions used by cumulus parameterizations. Mon Wea Rev 121:764–787

Grell GA, Dudhia J, Stauffer DR (1994) A description of the fifth generation Penn State/NCAR Mesoscale Model (MM5). NCAR Tech Note NCAR/TN- 398 + STR, 138 pp

Huffman GJ, Adler RF, Bolvin DT, Gu G, Nelkin EJ, Bowman KP, Hong Y, Stocker EF, Wolff DB (2007) The TRMM multi-satellite precipitation analysis: quasi-global, multi-year, combined-sensor precipitation estimates at fine scale. J Hydrometeor 8(1):38–55

Johnson RH, Houze RA (1987) Precipitating systems of the Asian monsoon. In: Chang CP, Krishnamurti TN (eds) Monsoon meteorology. Oxford University press, New York, pp 298–353

Juneng L, Tangang FT, Reason CJ, Moten S, Hassan WA (2007a) Simulation of tropical cyclone Vamei (2001) using the PSU/NCAR MM5 model. Meteorol Atmos Phys 97(1–4):273–290

Juneng L, Tangang FT, Reason CJ (2007b) Numerical case study of an extreme rainfall event during 9–11 December 2004 over the east coast Peninsular Malaysia. Meteorol Atmos Phys 98:81–98

Kain JS (2004) The Kain–Fritsch convective parameterization: an update. J Appl Meteor 43:170–181

Kain JS, Fritsch JM (1990) A one-dimensional entraining/detraining plume model and its application in convective parameterization. J Atmos Sci 47:2784–2802

Kain JS, Fritsch JM (1992) The role of the convective "Trigger Function" in numerical forecasts of mesoscale convective systems. Meteorol Atmos Phys 49:93–106

Kain JS, Fritsch JM (1993) Convective parameterization for mesoscale models: the Kain–Fritsch scheme. The representation of cumulus convection in numerical models. Meteor Monogr No. 46. Amer Meteor Soc, pp 165–170

Kerkhoven E, Gan TY, Shiiba M, Reuter G, Takana K (2006) A comparison of cumulus parameterization schemes in a numerical weather prediction model for a monsoon rainfall event. Hydrol Process 20:1961–1978

Kiehl JT, Hack JJ, Bonan GB, Boville BA, Williamson DL, Rasch PJ (1998) The National Center for Atmospheric Research Community Climate Model: CCM3. J Clim 11:1131–1149

Krishnamurti TN, Nam SL, Pasch RJ (1983) Cumulus parameterization and rainfall rates. Part II. Mon Wea Rev 111:815–828

Kuo HL (1965) On formation and intensification of tropical cyclone through latent heat release by cumulus convection. J Atmos Sci 22:456–475

Kuo HL (1974) Further studies of the parameterization of the influence of cumulus convection on large scale flow. J Atmos Sci 31:1232–1240

Kuo YH, Reed RJ, Liu Y (1996) The ERICA IOP 5 Storm. Part III: mesoscale cyclogenesis and precipitation parameterization. Amer Meteor Soc 124:1409–1434

Rakesh V, Singh R, Pal PK, Joshi PC (2007) Sensitivity of mesoscale model forecast during a satellite launch to different cumulus parameterization schemes in MM5. Pure Appl Geophys 164:1617–1637. doi:10.1007/s00024-007-0245-0

Ratnam VJ, Cox EA (2006) Simulation of monsoon depressions using MM5: sensitivity to cumulus parameterization schemes. Meteor Atmos Phys 93:53–78

Raymond DJ, Emanuel KA (1993) The Kuo cumulus parameterization. The representation of cumulus convection in numerical models. Meteor Monogr No. 24 Amer Meteor Soc, pp 145–147

Reynolds RW, Rayner NA, Smith TM, Stokes DC, Wang W (2002) An improved in situ and satellite SST analysis for climate. J Clim 15(13):1609–1625

Schultz P (1995) An explicit cloud physics parameterization for operational numerical weather prediction. Mon Wea Rev 123:3331–3343

Tangang FT, Juneng L, Reason CJC (2007) MM5 simulated evolution and structure of tropical cyclone Vamei (2001). Adv Geosci 9:191–207

Tangang F, Juneng L, Salimun E, Vinayachandran PN, Seng YK, Reason CJC Behera S, Yasunari T (2008) On the roles of the northeast cold surge, the Borneo vortex, the Madden–Julian Oscillation, and the Indian Ocean Dipole during the worst 2006/2007 flood in southern Peninsular Malaysia. Geophys Res Lett. doi:10.1029/2008GL033429

Vaidya SS (2006) The performance of two convective parameterization schemes in a mesoscale model over the Indian region. Meteor Atmos Phys 92:175–190

Wang W, Seaman NL (1997) A comparison study of convective parameterization schemes in a mesoscale model. Mon Wea Rev 125:252–278

Willmott CJ (1982) Some comments on the evaluation of model performance. Bull Am Meteorol Soc 63:1309–1313

Yang MJ, Tung QC (2003) Evaluation of rainfall forecasts over Taiwan by four cumulus parameterization schemes. J Meteor Soc Jpn 81:1163–1183

Zhang DL, Anthes RA (1982) A high-resolution model of the planetary boundary layer sensitivity tests and comparisons with SESAME-79 data. J Appl Meteor 21:1594–1609